CHEMIJA. 2020. Vol. 31. No. 1. P. 25–41

Sol–gel synthesis of calcium phosphate-based coatings – A review

Kunio Ishikawa[1],

Aivaras Kareiva[2*]

[1] *Department of Biomaterials, Faculty of Dental Science, Kyushu University, 3-1-1 Maidashi, Higashi-Ku, Fukuoka 812-8582, Japan*

[2] *Institute of Chemistry, Vilnius University, 24 Naugarduko Street, 03225 Vilnius, Lithuania*

Calcium phosphate (CP)-based biomaterials, especially nanostructured ones, show a high biocompatibility and increased biological properties. The coatings composed of stoichiometric hydroxyapatite have been extensively used to improve integration of metallic implants in the host bone. However, these coatings exhibited several drawbacks that limited their successful application. It was concluded in numerous articles that the sol–gel derived coatings can undergo cracking and delamination and are scarcely uniform. In this review article the recent advances on the sol–gel synthesis of different phosphate coatings and thin films are summarized. The attention is paid to coatings and thin films of calcium hydroxyapatite (CHAp), other phosphates, bioglasses and different composite materials. The state of the art, limitations, potentialities, open challenges, and the future scenarios for the application of CP bioceramics are highlighted in this study.

Keywords: calcium phosphates, calcium hydroxyapatite, bioglasses, composites, coatings, sol–gel processing

INTRODUCTION

Calcium phosphates (CP) are very important synthetic biomaterials due to their high bioactivity in human bones and dental tissues. These CP bioceramics are widely used to treat bone defects due to their chemical similarity to bone minerals with a good biocompatibility [1–6]. The nanodimensional forms of CPs can be utilized in biomineralization and as biomaterials also due to their excellent biocompatibility [7, 8]. Among nanomaterials, nanocalcium hydroxyapatite (n-CHAp) has been widely used in scaffolds for bone tissue engineering as well as implant coating material [8, 9]. Many bioactive glasses (BG), glass ceramics (GC) and nanocomposites have been prepared by various techniques during last decades [10–12].

Up to now, there are enormous efforts to develop different coatings that can enhance the biocompatibility properties of metallic implant materials and even provide antimicrobial effects [13–19]. The field of bone regeneration has pushed towards an extensive use of CHAp coated implants as a bone substitute, in view of its similarity to the inorganic phase of mineralized tissues. However, clinical results obtained by these traditional coatings are not as promising as expected, since due to a relatively high thickness, the synthesized coatings have a high tendency to cracking and delamination [18]. The quality of synthetic biomaterials, however, is highly dependent on the overall characteristics and properties of the synthesized products, such as phase purity and composition, crystallinity, pore size, particle size, particle-size distribution, particle morphology and a specific surface area [20]. Thus, all mentioned properties

* Corresponding author. Email: aivaras.kareiva@chgf.vu.lt

of bioceramics are highly sensitive to the processing conditions [21–36]. Over the last few decades, the sol–gel techniques have been used to prepare a variety of mixed-metal oxides, nanomaterials, nanoscale architectures, organic-inorganic hybrids, nanocoatings, glasses, monolithic, structured, composite and bio-inspired materials in the form of thin films [37–64].

In this study we present the results of a systematic analysis of the environment-friendly sol–gel synthetic approach to calcium phosphate coatings and thin films, including bioglasses and different composites. This review focuses on the sol–gel performance for biomaterials used for different purposes of clinical applications in orthopedic surgery, restorative dentistry and implantology, and discussing possible future strategies for the development of sol–gel processing for novel biomaterials with enhanced properties.

CALCIUM HYDROXYAPATITE COATINGS

Sol–gel synthesis using organic precursors

In 1998, Gross et al. [65] showed that calcium hydroxyapatite (CHAp) coatings could be successfully synthesized through the sol–gel technique, using calcium diethoxide and triethyl phosphite dissolved in ethanol as starting materials. 1,2-ethanediol was used as a complexing agent in the sol–gel processing. It was concluded that the production of thin homogeneous hydroxyapatite coatings by the sol–gel method on titanium substrates using alkoxide precursors required control of the aging time and annealing temperature. Interestingly, the CHAp powders through the sol–gel technique using alkoxides as starting materials for the first time were obtained in 1990 [66]. One year later the same synthetic approach was used to fabricate CHAp coatings on glass, polycrystalline alumina, partially stabilized zirconia, Ti6Al4V alloy and single crystal MgO substrate materials [67]. It was determined that coating thickness varied between 70 and 1000 nm depending on the number of applied layers. SEM and AFM examination revealed the presence of two distinct regions consisting of grains 200 and 800 nm in size, respectively, after being sintered at 1000°C.

However, the alkoxide route was soon slightly modified using a calcium inorganic precursor. Calcium nitrate ($Ca(NO_3)_2 \cdot 4H_2O$) has been selected as a calcium precursor for the synthesis of calcium hydroxyapatite when the organic phosphorous precursor, triethyl phosphite, was used in the sol–gel processing [68]. The mechanisms of on-going hydrolysis/condensation/polymerization processes resulting in the formation of more (-Ca–O–P-)-containing bonds in dry gels were suggested. Upon ageing, the hydrolyzed phosphorus sol $PHO(OEt)_2$ or $P(OEt)_{3-x}(OH)_x$ interacted with calcium sol, possibly in the form of $Ca(OEt)_y(NO_3)_{2-y}$ in anhydrous ethanol and Ca^{2+} in water, to form oligomeric derivatives containing Ca–O–P bonds. For the ethanol-based process, the reaction may proceed as follows:

$$P(OEt)_{3-x}(OH)_x + Ca(OEt)_y(NO_3)_{2-y} \rightarrow (OEt)_y(NO_3)_{2-y} - \\ - Ca\text{-}O\text{-}HPO(OEt)_{3-x} + H_2O + C_2H_5OH. \quad (1)$$

The low temperature (375°C) fabricated CHAp coatings on the Ti implant demonstrated bioactivity over a short time of the period incubation in the simulated body fluid (SBF) at ambient temperature.

The simplified sol–gel synthesis approaches for the preparation of CHAp coatings on galvanostatically treated stainless steel and NiTi alloy substrates were used by Ak Azem and Cakir [69] and Zhang et al. [70], respectively. They did not use any complexing agent in the sol–gel processings. Figure 1 shows the comparison of the XRD patterns for the CHAp coatings obtained at different processing conditions. The results summarized in the article [69] revealed that the coating derived

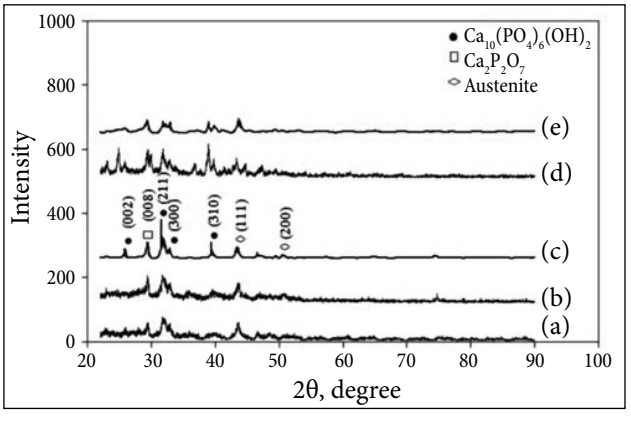

Fig. 1. XRD patterns of CHAp coatings obtained on 316L stainless steel substrates with sols aged for different time [69]

from the sol with the aging time of 24 h shows better crystalline properties and surface morphology that has a dense structure with a low crack density. Acidic conditions of the used sol solutions excite the formation of the impurity phase of $Ca_2P_2O_7$. It was shown that modification of the substrate surface with electrochemical seeding helped to develop better adherence of the CHAp film on to the surface when compared to those without seeding. It is interesting to note that the CHAp coating, with a thickness at a sub-micron scale, has been formed not only on the surface of the porous NiTi alloy but also inside the pores without blocking them [70].

2.2. Sol–gel synthesis using only inorganic precursors

Many authors suggested for the synthesis of CHAp coatings and thin films by a sol–gel method to use phosphorous pentoxide (P_2O_5), phosphoric acid (H_3PO_4), ammonium hydrogen phosphates ($(NH_4)_2HPO_4$) or sodium phosphate (Na_3PO_4) and calcium nitrate tetrahydrate ($Ca(NO_3)_2{\cdot}4H_2O$), calcium acetate monohydrate ($Ca(CH_3COO)_2{\cdot}H_2O$) or calcium chloride ($CaCl_2$) as starting materials [71–83]. The sol–gel chemistry routes have been developed to prepare calcium hydroxyapatite thin films on titanium, silicon, silica and stainless steel substrates by dip-coating and spin-coating techniques. The quartz substrates were coated 1, 5, 15 and 30 times using both, dip- and spin-coating techniques and annealed at 1000°C after each dipping or spinning procedure [75]. It was demonstrated that the crystallization of calcium hydroxyapatite depends on the number of layers. The progressive changes in the surface morphology of CHAp films with increasing the dipping or spinning time were detected (Fig. 2). The SEM micrographs of sol–gel calcined at 1000°C showed highly uniform and crystalline particles with

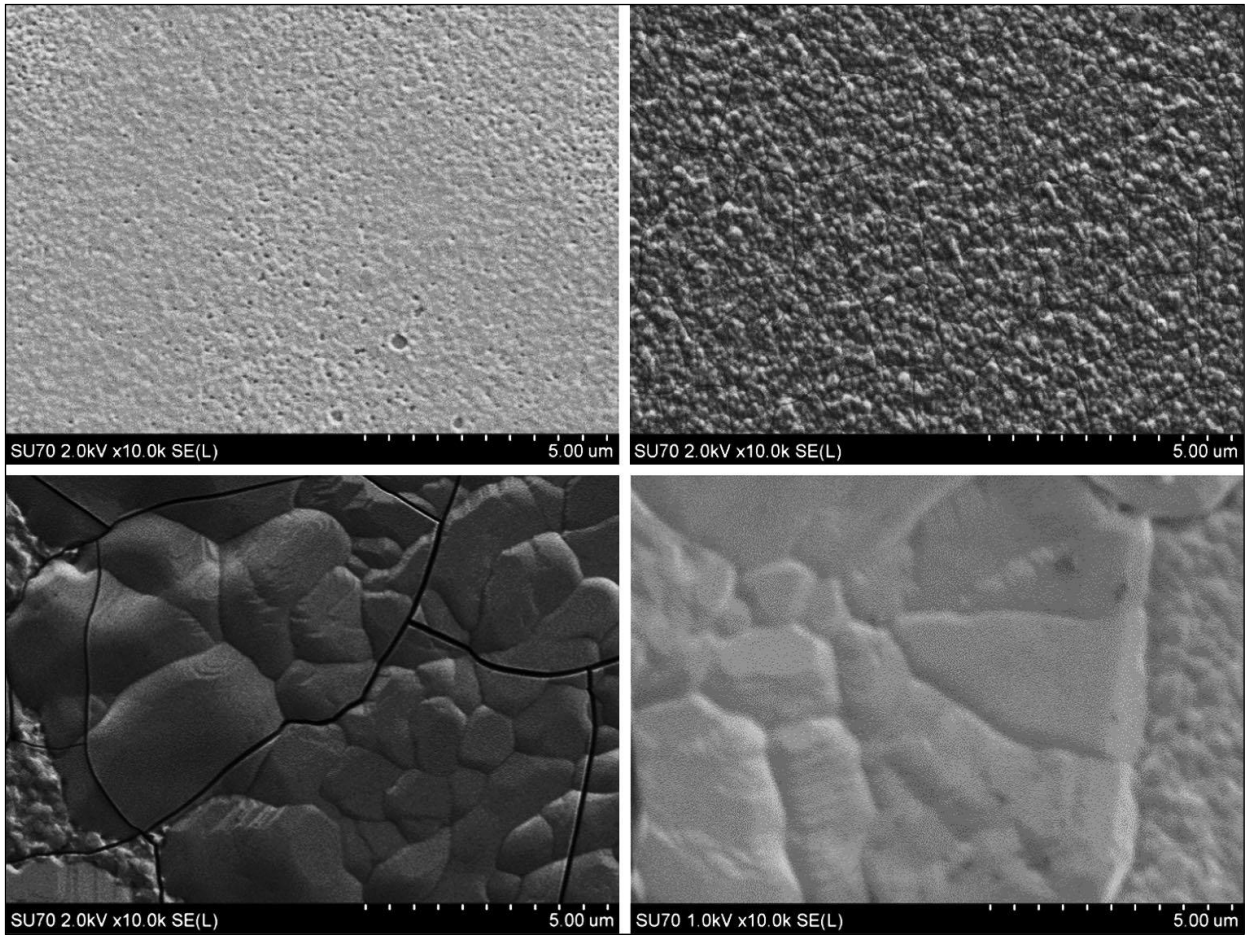

Fig. 2. SEM micrographs of the CHAp samples containing 1 layer (at top, at left), 5 layers (at top, at right), 15 layers (at bottom, at left) and 30 layers (at bottom, at right) of Ca–P–O gel deposited by spin-coating technique and calcined at 1000°C [75]

smooth surfaces. The homogeneous CHAp coatings of regular polygons with a narrow particle size distribution (300–400 nm) have formed in the samples prepared with 15 and 30 spinning and annealing procedures. The highest roughness (44.2 at a surface area of 2/2 μm) was observed in the sample containing 30 layers. The thickness of the CHAp films increased monotonically with increasing the number of spin-coating and annealing procedures.

The calcium hydroxyapatite thin films on silicon substrate were synthesized using only a spin-coating procedure [77]. The results of Raman spectroscopy showed the peak at 961 cm^{-1}, which corresponds to the symmetric stretching vibration of phosphate groups in calcium hydroxyapatite proving the formation of high quality CHAp thin films on the Si substrate obtained using an aqueous sol–gel chemistry approach. The Raman spectra in the wavenumber region from 600 to 1250 cm^{-1} of the Si substrate and the CHAp sample containing 30 layers are presented in Fig. 3. It was proposed from the Fourier transform infrared (FTIR) spectroscopy results that formation of the oxyhydroxyapatite $Ca_{10}(PO_4)_6(OH)_{2-2x}O_x$ phase on the Si substrate was also possible [78].

The authors [76] showed that the sol–gel-derived hydroxyapatite-coating layer on the Co-Cr-based substrate, dip-coated with two different thicknesses, after the sintering process exhibited a significant improvement in corrosion resistance compared with the uncoated material. The potentiodynamic polarization test in SBF at 37°C confirmed that the thickness of the CHAp-coating layer affected the corrosion rate of the substrate.

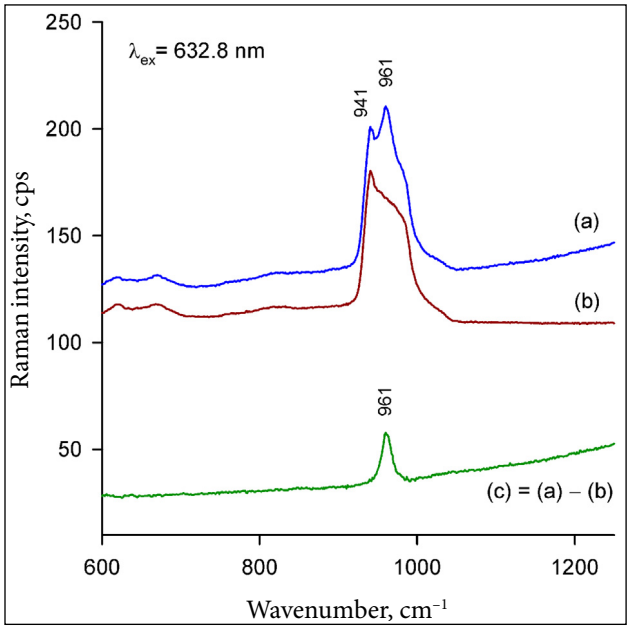

Fig. 3. Raman spectra of the CHAp sample obtained with 30 layers on Si substrate (a) and only pure Si substrate (b). Difference of two spectra (c) is also shown [77]

An aqueous sol–gel method was developed for the synthesis of calcium hydroxyapatite ($Ca_{10}(PO_4)_6OH_2$, CHAp) thin films on the stainless steel substrate at 1000°C temperature with a low number of layers [74]. It was demonstrated that the values of the contact angle on the surface of films decreased dramatically in comparison with the pure substrate. Thus, high hydrophilicity CHAp coatings were obtained after five immersing, withdrawal and annealing procedures in the sol–gel processing. The CHAp coatings on the stainless steel substrate with a considerably increased phase purity and homogeneity have been synthesized with increasing the number of immersing, withdrawal and annealing procedures [79]. The SEM results indicated a slightly different surface morphology of the spin-coated and dip-coated samples when a large number of CHAp layers was designed. The spin-coated samples were homogeneous and composed of nano-scaled particles. The individual particles were about 100–300 nm in size. The hydrophilic CHAp coatings with contact angle values of 78.8°–82.8° were obtained after 30 immersing, withdrawal and annealing procedures in the sol–gel processing (see Fig. 4).

To increase the surface quality of CHAp coatings the specific modification of the surface of titanium and stainless steel substrates before the coating procedures was performed [80, 82]. To deposit calcium titanate sublayers by a sol–gel route, titanium (IV) isopropoxide and either calcium acetate monohydrate or calcium hydroxide were used as Ti and Ca sources, respectively. Figure 5 shows a schematical view of sol–gel preparation of calcium titanate sublayers and calcium hydroxyapatite thin films on the Ti substrate. In the XRD patterns recorded peaks attributable to $CaTiO_3$ were clearly, however, along with $CaTiO_3$, TiO_2 was also present at the Ti surface. Moreover, it was observed that the intensity of TiO_2 reflections increased with each step of dipping in the CHAp gel procedure. Thus, the initial

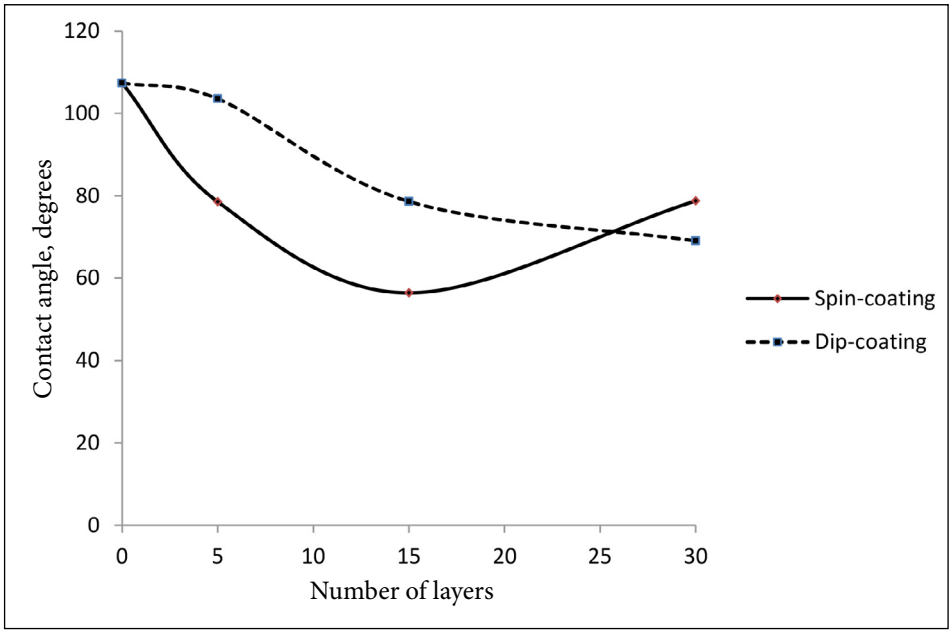

Fig. 4. The results of contact angle measurements for the sol–gel derived CHAp coatings [79]

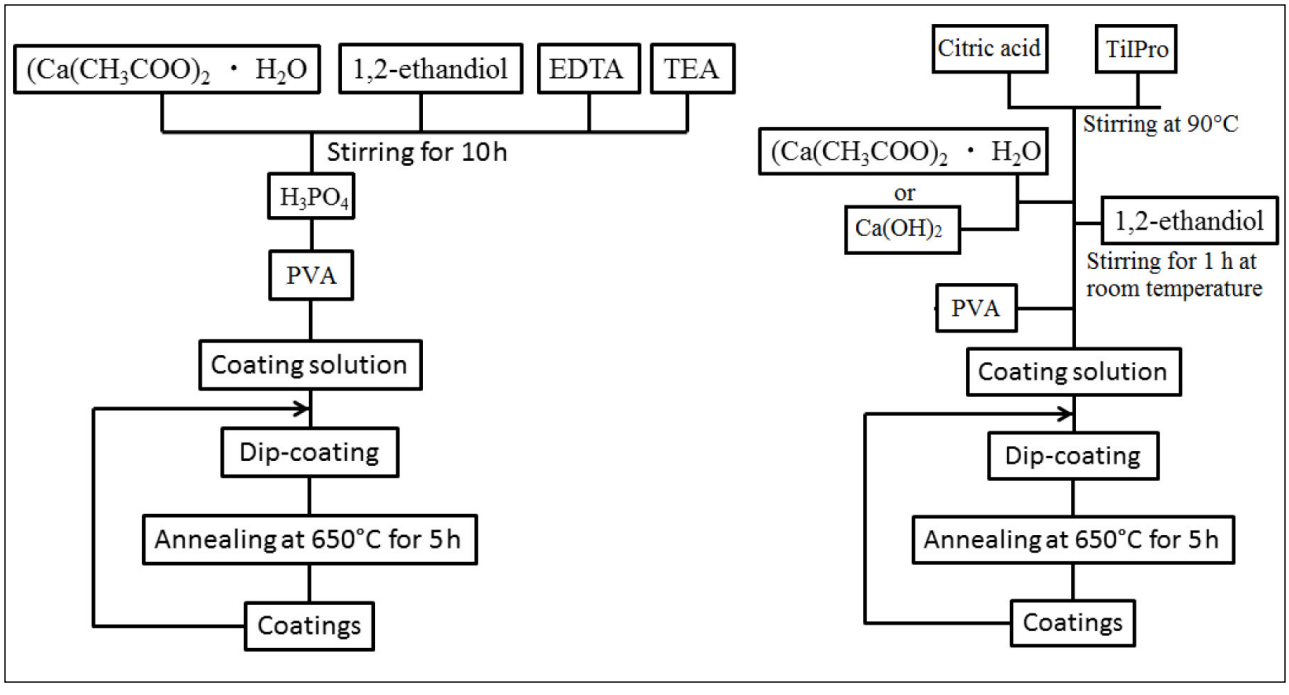

Fig. 5. Schematical diagrams of the sol–gel preparation of calcium titanate sublayers (left) and calcium hydroxyapatite thin films (right) on Ti substrate [80]

formation of a sublayer of calcium titanate on the Ti substrate did not prevent the formation of titanium oxide. The situation was different when the Ti substrate was pre-heated before the formation of a calcium titanate sublayer. The intensities of the diffraction peaks of TiO_2 remained unchanged with increasing the number of CHAp layers up to 20 (see Fig. 6).

An aqueous sol–gel method was applied for the synthesis of CHAp thin films on medical grade stainless steel substrates with a transverse and longitudinal patterned roughness. A schematic diagram of the preparation of CHAp coatings is presented in Fig. 7. The surface of CHAp coatings on the roughened stainless steel substrate obtained after 25 spin-coating procedures was composed of

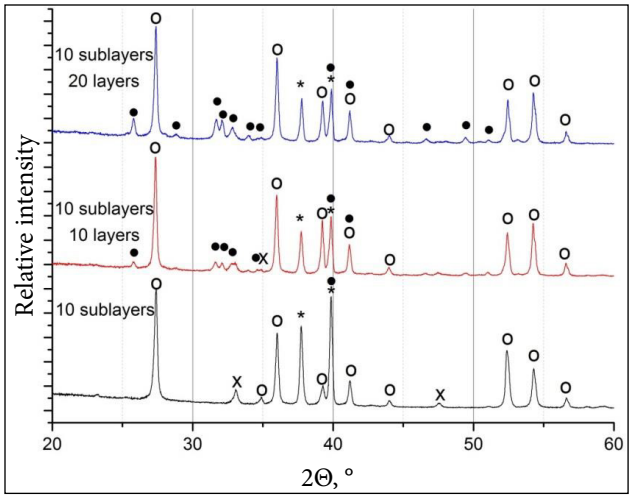

Fig. 6. XRD patterns of CHAp films on Ti (initially pre-heated) with the $CaTiO_3$ sublayer (derived from calcium acetate) annealed at 650°C for 5 h in air. Diffraction peaks are marked as follows: • – ($Ca_{10}(PO_4)_6(OH)_2$ (PDF: 74-0566); o – TiO_2 (PDF: 77-2224); * – Ti (PDF: 44-1294); x – $CaTiO_3$ (PDF: 22-0153) [80]

homogeneously distributed well-interconnected spherical grains about 250 nm in size. The formed layer of calcium hydroxyapatite was continuous and pore-free. The increased hydrophobicity of CHAp coatings on the rough substrate due to the synergy of energetic and chemical effects, however, was determined [82]. In this study, the fabricated CHAp coatings were estimated after immersing in SBF for 2, 3 and 4 weeks. After 1 month of soaking in SBF, a decrease in the intensity of the peaks attributable to both CHAp and TCP phases was observed. The XRD results clearly indicated that amorphous calcium phosphate had formed on the immersed samples.

The CHAp coatings were fabricated from the Ca–P–O sol–gel solution for the first time on the silicon nitride (Si_3N_4) substrate [81]. It was observed that the formation of CHAp as a single phase occurred after annealing of the coatings in air atmosphere at 650°C for 5 h. The CHAp coatings obtained after 30 dip-coating cycles were slightly cracked and porous, having a smoother surface without formation of islands. The Raman data indicated that the studied samples possess a hydroxyapatite molecular structure and no formation of oxyhydroxyapatite $Ca_{10}(PO_4)_6(OH)_{2-2x}O_x$ on silicon nitride was observed. Usinskas et al. [83] have fabricated calcium hydroxyapatite thin layers from the Ca–P–O sol–gel solution on the silicon (Si) substrate using the improved dip-coating method. This developed technique allowed them to achieve the desired results 4 times faster in comparison with the previously suggested processing.

Based on these observations and characterization, it may be concluded that the sol–gel method provides an effective way to produce CHAp coatings on a variety of substrates with the enhanced apatite forming ability beneficial for biomedical applications. Such CHAp coated specimens could be very important implantable materials and used as substitute material for human hard tissues (bones and teeth).

2.3. Sol–gel synthesis of cation-substituted CHAp layers

Metal-substituted $Ca_{10}(PO_4)_6(OH)_2$ coatings were also synthesized by sol–gel synthesis routes [84–91]. The inhibitory and antimicrobial effects of silver particles have been known since ancient times, however, possible antimicrobial properties of calcium hydroxyapatite doped with silver were announced almost 15 years ago [92]. The cytotoxicity and antimicrobial effects were observed by authors in the Ag-doped bulk CAHp prepared using different techniques. Later, Buckley et al. [93] used Ag-doped mesoporous CHAp with a high surface area as biocompatible supports for antibacterial applications. In the first investigation of Ag-doped CHAp coatings [84], the prepared Ag-CHAp sol was coated on

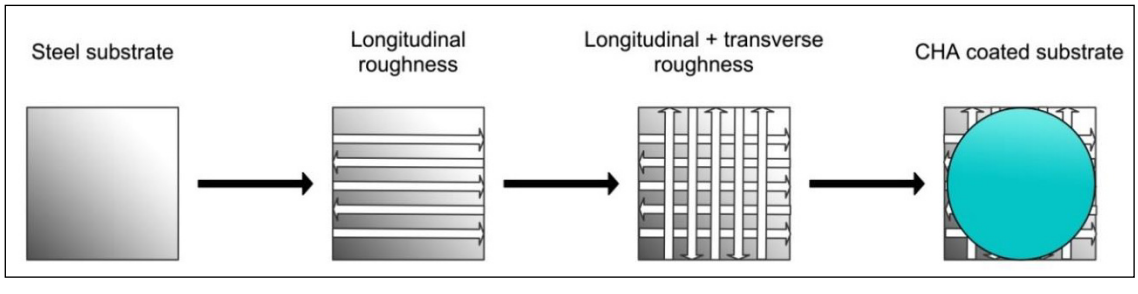

Fig. 7. A schematic diagram of the preparation of CHAp coatings [82]

passivated Ti surfaces by spin coating at 5000 rpm for 50 s. The coated-Ti surfaces were immediately dried at 70°C and then heat-treated at 650°C for 3 h. The Ag-CHAp sol was prepared by reacting calcium nitrate tetrahydrate with methyl alcohol to produce calcium precursors. Phosphorus precursors were also prepared by reacting triethyl phosphite in 0.03 mL acetic acid (CH_3COOH). The two precursors were then mixed with silver nitrate ($AgNO_3$) powders and 0.1 mol of the so-called drying control chemical additive (DCCA). The determined values of contact angles for the Ag-CHAp coatings confirmed a high hydrophilic character of the obtained thin films. Besides, the *in vitro* bacterial adhesion study indicated a significantly reduced number of *S. epidermidis* and *S. aureus* on the Ag-CHAp surface. The Ag-CHAp coating for implants fabricated by immersing the bioglass coatings to the simulated body fluid under hydrothermal conditions showed antibacterial activity against *Staphylococcus aureus* and *Escherichia coli* [90].

It is well known that co-doped CHAp scaffolds exhibited synergetic effects with enhanced antibacterial properties as well [94–99]. Therefore, the CHAp coating by a simultaneous incorporation of Ag^+ and Zn^{2+} ions to study a cumulative effect of dopants was also synthesized using the sol–gel technique [89]. The CHAp coatings were synthesized using calcium nitrate tetrahydrate and phosphor pentoxide as Ca and P precursors, respectively. Zinc nitrate hexahydrate and silver nitrate were used to substitute for Ca in the CHAp structure. The obtained sols were aged for 48 h. Glass substrates were immersed into clear and stable sols, withdrawn at a speed of 4 cm/min. Each coating was dried at 75°C and coating steps were repeated for 5 times. The coated specimens were heat-treated at 600°C for 2 h in air. It was demonstrated that the CHAp structure was formed successfully without the formation of undesirable phases such as $CaCO_3$, CaO, $Ca_2P_2O_7$ and $CaHPO_4$. Also, other calcium phosphate compositions with the exception of β-tricalcium phosphate (β-TCP) were not observed. The possible cationic substitution mechanism in CHAp could be expressed by the following equation:

$$Ca_{10}(PO_4)_6(OH)_2 + 2xAg^+ \rightarrow 2\ Ca_{10-x}Ag_{2x}(PO_4)_6(OH)_2 + xCa^{2+}, \quad (2)$$

$$Ca_{10}(PO_4)_6(OH)_2 + xZn^{2+} \rightarrow 2\ Ca_{10-x}Zn_x(PO_4)_6(OH)_2 + xCa^{2+}. \quad (3)$$

It was concluded that the CHAp coatings containing 1.0 wt.% Zn – 0.9 wt.% Ag in the composition had better surface characteristics. The colony count showed that bacterial colonies on the Zn–Ag substituted CHAp surface decreased significantly.

Magnesium is one of the most important divalent ions associated with biological apatite. In [85, 88] series of magnesium-substituted calcium hydroxyapatite $Ca_{10-x}Mg_x(PO_4)_6(OH)_2$ coatings were synthesized onto the Ti6Al4V substrate by the sol–gel dip-coating method to determine how magnesium influences the synthesis and the resulting structural and biological properties. Calcium nitrate tetrahydrate, phosphorus pentoxide and magnesium nitrate hexahydrate were selected to prepare Ca-, P- and Mg-precursors, respectively, in this study. Fig. 8 shows the typical SEM micrographs of MG63 cells after

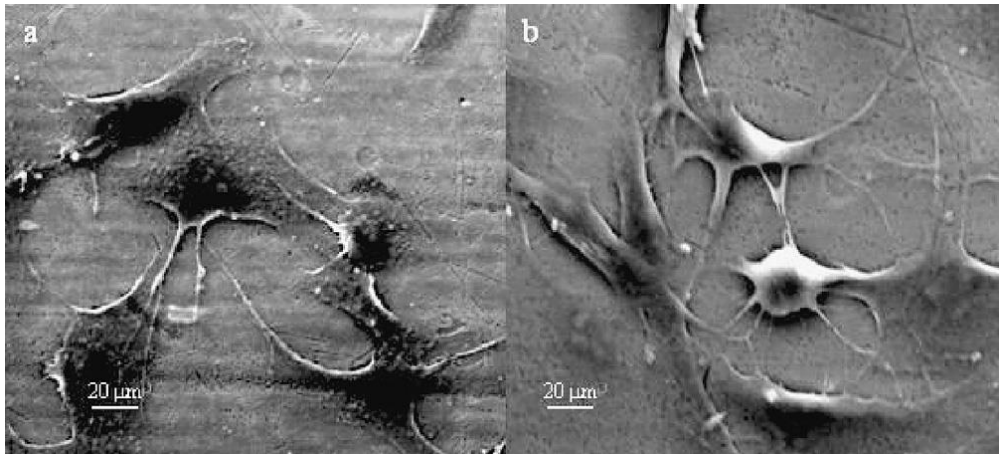

Fig. 8. Typical morphology of cells attached on the apatite coatings: (a) CHAp and (b) Mg-CHAp [85]

1 day of culture on the surface of the CHAp and Mg-CHAp coatings. It could be observed that all the cells are attached to the coating surfaces and spread well. Cell proliferation was also directly monitored by counting cell numbers at culture periods.

Taken together, all these findings suggested that the CHAp coatings with incorporated different cations into the apatite structure showed slightly different morphologies and can yield safe and highly effective surfaces for metallic implants.

COATINGS OF OTHER CALCIUM PHOSPHATES

Different calcium phosphate ceramics have been also applied in dentistry, orthopedics and surgery for about three decades because of their chemical similarity to the mineral component of calcified tissues [100–104]. Biphasic calcium phosphate (BCP) ceramic comprises a mixture of CHAp and β-TCP. This material was regarded as suitable for synthetic bone applications and has been extensively used as substitution materials for artificial bone grafts [105–108]. During calcination of the amorphous gels the crystalline phase of BCP is forming:

$$10\ Ca(NO_3)_2 + 6\ (NH_4)_2HPO_4 + 8\ NH_4OH \rightarrow Ca_{10}(PO_4)_6(OH)_2 + 20\ NH_4NO_3 + 6\ H_2O, \quad (4)$$

$$3\ Ca(NO_3)_2 + 2\ (NH_4)_2HPO_4 + 2\ NH_4OH \rightarrow Ca_3(PO_4)_2 + 6\ NH_4NO_3 + 2\ H_2O, \quad (5)$$

$$9\ Ca(NO_3)_2 + 6\ (NH_4)_2HPO_4 + 6\ NH_4OH \rightarrow Ca_9(HPO_4)(PO_4)_5OH + 18\ NH_4NO_3 + 5\ H_2O, \quad (6)$$

$$Ca_9(HPO_4)(PO_4)_5OH \rightarrow 3\ Ca_3(PO_4)_2 + H_2O. \quad (7)$$

Gan and Pilliar [109] have prepared CP thin films on sintered porous-surfaced Ti6Al4V alloy implants by the sol–gel method using either an inorganic precursor solution (with calcium nitrate tetrahydrate and ammonium dihydrogen phosphate) or an organic precursor solution (with calcium nitrate tetrahydrate and triethyl phosphite). It was determined that both approaches resulted in the formation of nanocrystalline carbonated hydroxyapatite ($Ca_{10-x/2}(PO_4)_{6-x}(CO_3)_x(OH)_2$, CHA) [110] films but with different Ca/P ratios and structures. For instance, the inorganic route-formed film had a lower Ca/P ratio (1.46 cf 2.10 for the organic route-formed film). Moreover, small cracks of CP thin films were noted in the sintered neck regions of Ti6Al4V alloy implants (Fig. 9).

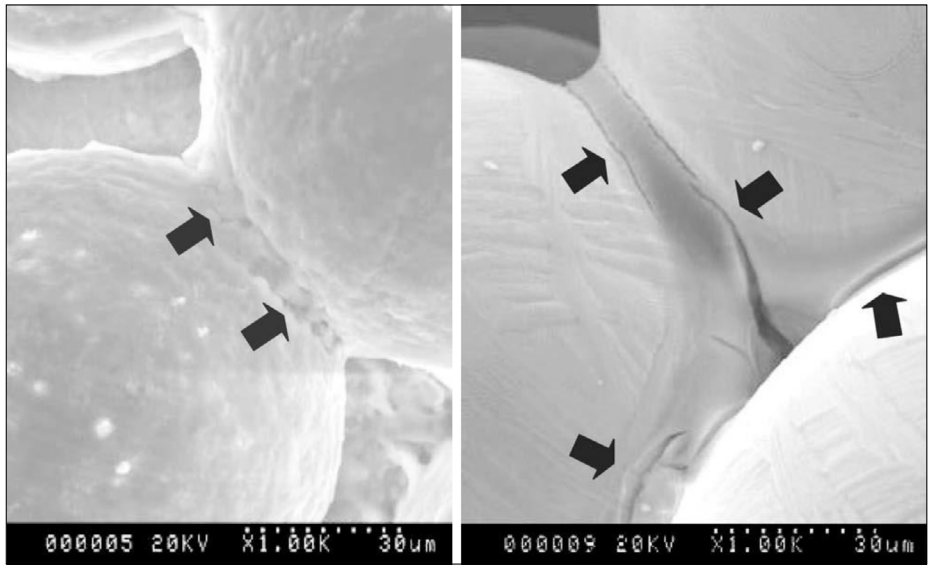

Fig. 9. SEM micrographs of the Ca–P coated implant formed using the inorganic (left) and organic (right) routes. Arrowheads indicated the cracks in the sintered neck regions [109]

An aqueous sol–gel method for the preparation of biphasic calcium phosphate/calcium hydroxyapatite thin films on titanium substrate using the dip-coating technique has been developed by Stankeviciute et al. [111]. The schematic diagram used for the preparation of Ca–P–O sol is presented in Fig. 10. The standard immersing (85 mm/min) and withdrawal rates (40 mm/min) for the dip-coating process (20 s) were applied for all the samples. The dipping procedure was repeatedly performed 5, 15 and 30 times. After evaporation of the solvent, the substrates were dried in an oven at 110°C and heated at 1000°C for 5 h with a heating rate of 1°C/min. The formation of small and very homogeneously distributed spherical particles with an average grain size of 200 nm was observed for the coatings with 15 layers (see Fig. 11). As also seen, the coatings of 30 layers had similar structural characteristics. However, the size of spherical particles increased significantly up to 0.6–0.8 μm. It was concluded that the SEM micrographs of Ca–P–O gels calcined at 1000°C showed the formation of highly uniform and crystalline particles with smooth surfaces. There were no macro cracks or pores too.

The BCP coatings have been successfully prepared on the Nitinol foil (with the wt.% content of 55.82 Ni, ≤0.20 other metal impurities, and balance Ti) via the organic-based sol–gel method [112]. In the sol–gel synthesis calcium 2-ethylhexanoate was dissolved in ethylhexanoic acid. The above solution was mixed with 2-ethylhexylphosphate, and the obtained sol was stirred at room temperature for 4 h before being used for coating. The coating was performed by dipping the substrates into the CaP sol, pulling them out at a speed of approximately 6 cm min^{-1}, drying in air at 130°C, and calcining in a preheated furnace at 600°C for 10 min. The multilayered coatings on Nitinol were prepared by cycling the above procedure. The authors concluded that the sol–gel method offered the opportunity to form biphasic CaP coatings on metallic implants and to create a grafting material with high bioactivity and bioresorbility for medical applications.

Dikici et al. [113] suggested a rather complicated procedure to synthesize precursor gels for the preparation of the BCP coatings on the Ti–29Nb–13Ta–4.6Zr (TNTZ) alloy substrates, despite this very simple starting materials $Ca(NO_3)_2{\cdot}4H_2O$ and $(NH_4)_2HPO_4$) were used. An ultrasonic homogenizer was used to prepare suitably stabilized gels. The viscosities of the gels after optimization of the homogenization time and power duty were measured as 37 and 41 (±2) centipoise (mPa s). The substrates were immersed in the solution for 5 min, dried at 200°C in air, and followed by sintering at 750°C. The effective coating thickness was measured as ~10 μm (±3) in all coatings.

In conclusion, the properties of metallic implants could be upgraded upon surface modification with CaP using suitable surface modification techniques [114]. However, some features of sol–gel

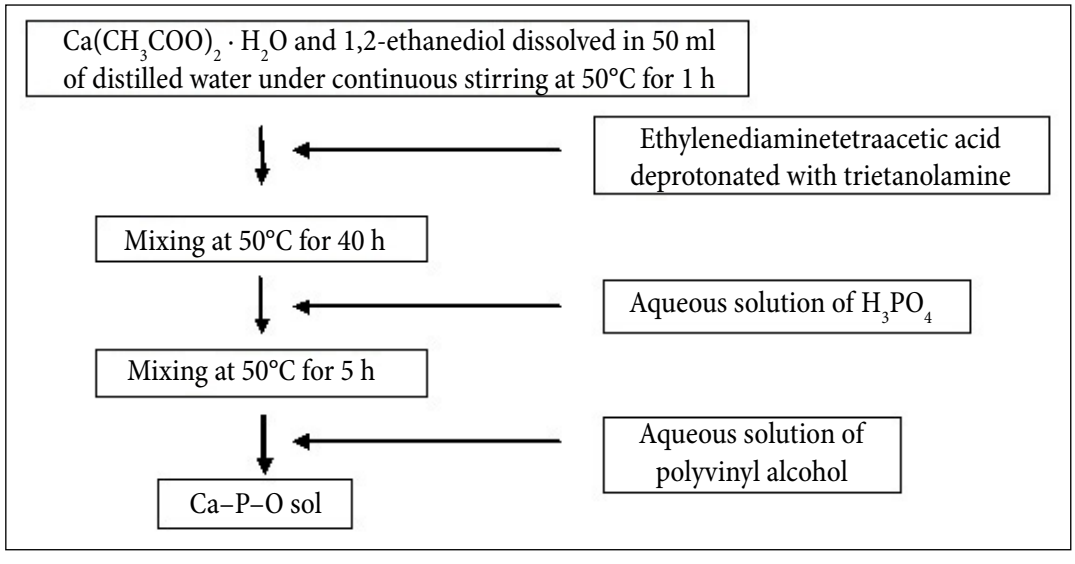

Fig. 10. The schematic diagram used for the preparation of Ca–P–O sol [111]

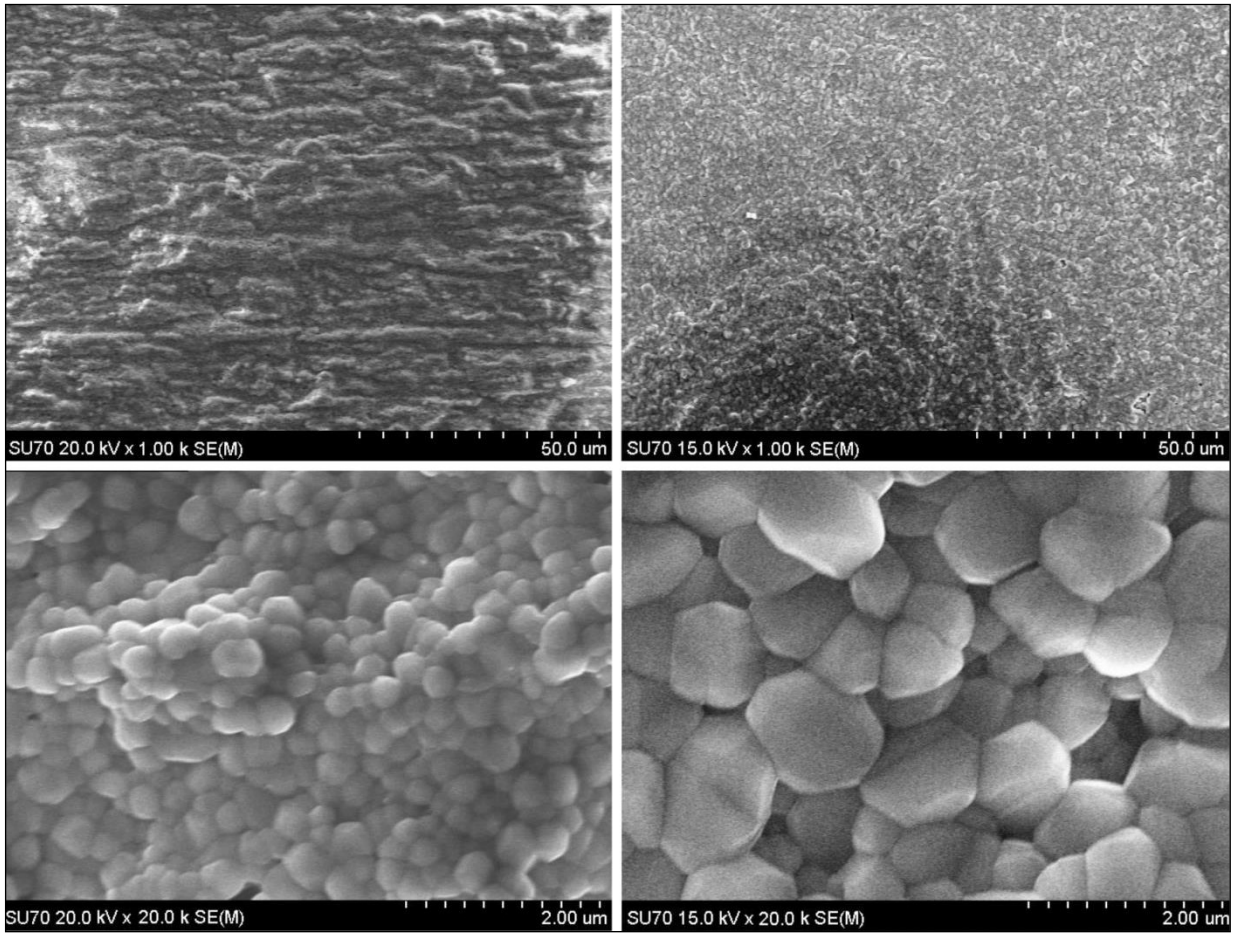

Fig. 11. SEM micrographs of BCP fabricated on the Ti substrate by an aqueous sol–gel method [111]

synthesis of CP coatings, such as simplicity of preparation, cost effectiveness and possibility to prepare a highly adherent microporous layer, which is of prime importance for clinical purposes, should be established in the next few years.

COATINGS OF CALCIUM PHOSPHATE GLASSES

It is well known that the sol–gel method enables one to fabricate powdered bioglasses as well [115–118]. Wang et al. [119] have synthesized the first crack-free $CaO–P_2O_5–SrO–Na_2O$ glass-ceramic coatings on the Mg alloy substrate using the polyethyleneglycol (PEG) assisted sol–gel method followed by heat-treatment at 400°C. For dip-coating the solution of $Ca(NO_3)_2·4H_2O$, $Sr(NO_3)_2$, $NaNO_3$ and P_2O_5 in PEG was used. It was mentioned that the glass transition temperature of the calcium phosphate system has shifted to lower temperature (226°C) due to the addition of PEG, which promoted the crystal nuclei formation. The endothermal peaks visible in the DSC curves (Fig. 12) support this conclusion.

The sol–gel chemistry approach was suggested for the preparation of bioglass coatings also on the stainless steel substrate [120]. The coated systems were analysed *in vitro* by immersion in

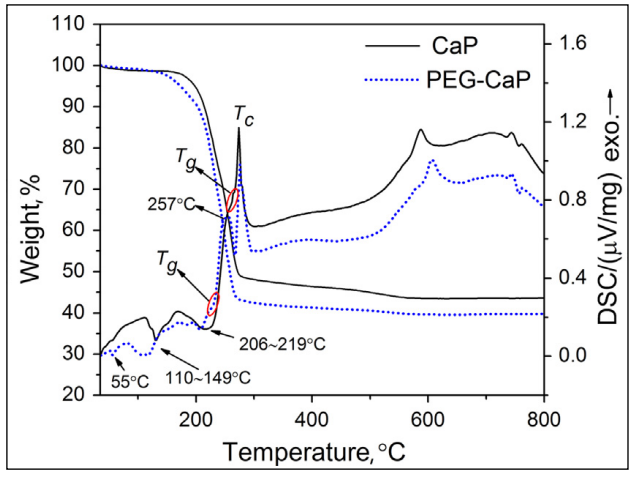

Fig. 12. DSC and TG curves of CP and PEG–CP xerogel powders [119]

a solution that simulates the inorganic concentration of ions in the human plasma. After immersing the samples in the SBF solution for 30 days, the coatings provided an enhanced corrosion resistance when compared with bare stainless steel in SBF, being potential films able to provide both corrosion resistance and bioactivity. It was confirmed by SEM and HRTEM that the newly grown bone tissue was identified around the implant growing in contact with the bone marrow.

The SiO_2·CaO·P_2O_5 glass coatings on glass coverslips substrates were synthesized by the sol–gel technique using a semi-alkoxide route [121]. In the sol–gel processing TEOS, $Ca(NO_3)_2$·$4H_2O$ and triethyl phosphate (TEP) were used as precursors of SiO_2, CaO and P_2O_5, respectively (see Fig. 13).

The phosphate-based glass coatings were also soaked in SBF for the *in vitro* bioactivity test. The formation of typical globules with the morphology characteristic of the bonelike apatite, which precipitates on bioactive materials when they are soaked in the SBF solution, was observed. Such observations were widely reported in the literature as well [122–124]. It was determined that the BET surface area increases with the silica content of the glass, and it is also enhanced by the presence of magnesium. When the dense glass ceramic samples were soaked into the SBF solution, the formation of apatite-like layers was detected. The random-sized particles with a spheroidal morphology were nucleated and formed onto the surface of bulk glass. The highest rate of apatite formation was observed on the glasses that do not contain magnesium. Partial replacement of calcium by magnesium, however, provoked a strong reduction in the initial crystal growth rate, but nevertheless a continuous increase of the apatite layer with time was observed in both cases. Silver doped-bioactive glass (SiO_2–CaO–P_2O_5–Ag_2O) coatings on the Ti substrate were recently fabricated by the sol–gel method using the dip-coating technique [125]. The same starting materials as in [121] along with $AgNO_3$ were selected. It was observed from the SEM micrographs that the precipitation of apatite crystals occurred on the coated samples after 14 days soaking in SBF.

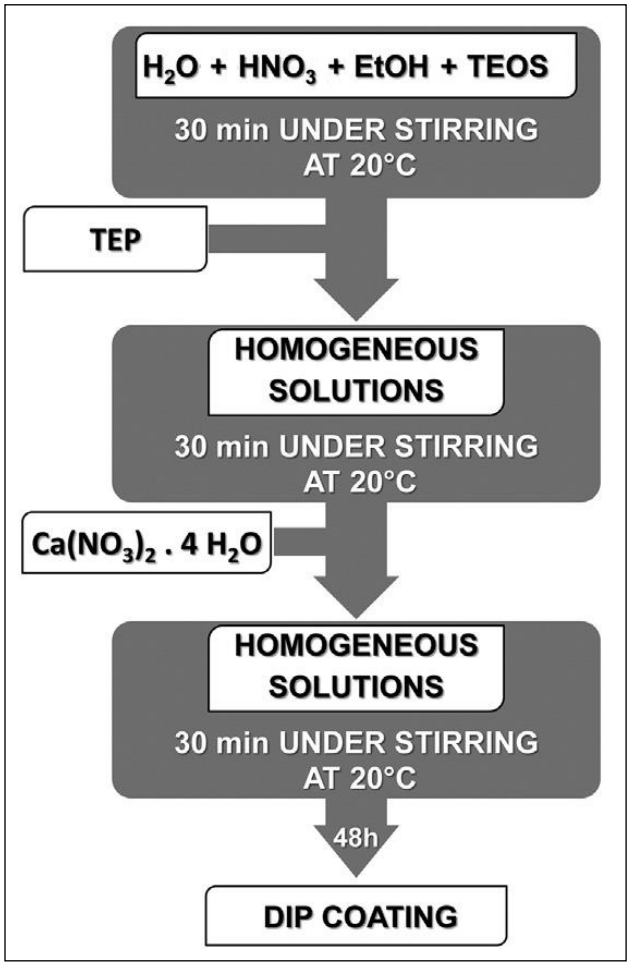

Fig. 13. Flow chart of the sol–gel synthesis and dip coating procedure [121]

The results summarized in this part are promising with respect to the application of sol–gel derived calcium phosphate silicate glasses as bioresorbable materials. The coatings of calcium phosphate glasses offer the possibility of bioactivation, corrosion protection and infection prevention of metallic implants. It is evident that such implanted materials could be successfully applied for new bone formation and have utility for cell-tracking applications in regenerative medicine.

CALCIUM AND PHOSPHORUS CONTAINING COMPOSITE COATINGS

Different composite materials have been used recently as promising bioactive materials with applications ranging from structural implants to tissue engineering scaffolds [126–133]. Sol–gel processing methodology for the production of fluorapatite–titania–carbon nanotubes (FCHAp–TiO_2–CNTs) nanocomposite coatings on the Ti–6Al–4V substrate has been developed by Sasani et al. [134]. The aims of this study were to investigate the role of decorated CNTs in the microstructural and

nanomechanical evolution of FCHAp-based composite coatings. The method consisted in the sol–gel synthesis of composite starting from the precursors tetraethylorthotitanate, calcium nitrate tetrahydrate and TEP dissolved in ethanol and mixing with CNTs. The obtained composite sol was allowed to age for 24 h. After the aging process, composite sols were directly spin-coated on Ti–6Al–4V. Nanomechanical evaluation of coatings showed that CNTs have a key role in improvement of mechanical properties. A similar synthesis approach was used later for the preparation of the silver/FCHAp composite on the Ti–6Al–4V substrate [135]. In order to prepare silver and fluoride doped hydroxyapatite sols, silver nitrate was added to the Ca-containing solution and ammonium fluoride was added to the P-containing solution, respectively. The final amount of silver in the Ag-CHAp samples was 0.3 wt.% and the ratio of [P]/[F] varied from 3 to 6. All the coatings were prepared by dipping titanium substrates at a withdrawal speed of 3 cm/min in the sols. Figure 14 shows the SEM micrographs of synthesized composite coatings. It was determined that the average thickness of coatings was 1.3 μm. As shown in Fig. 14c, d, the Ag-1FCHAp coating

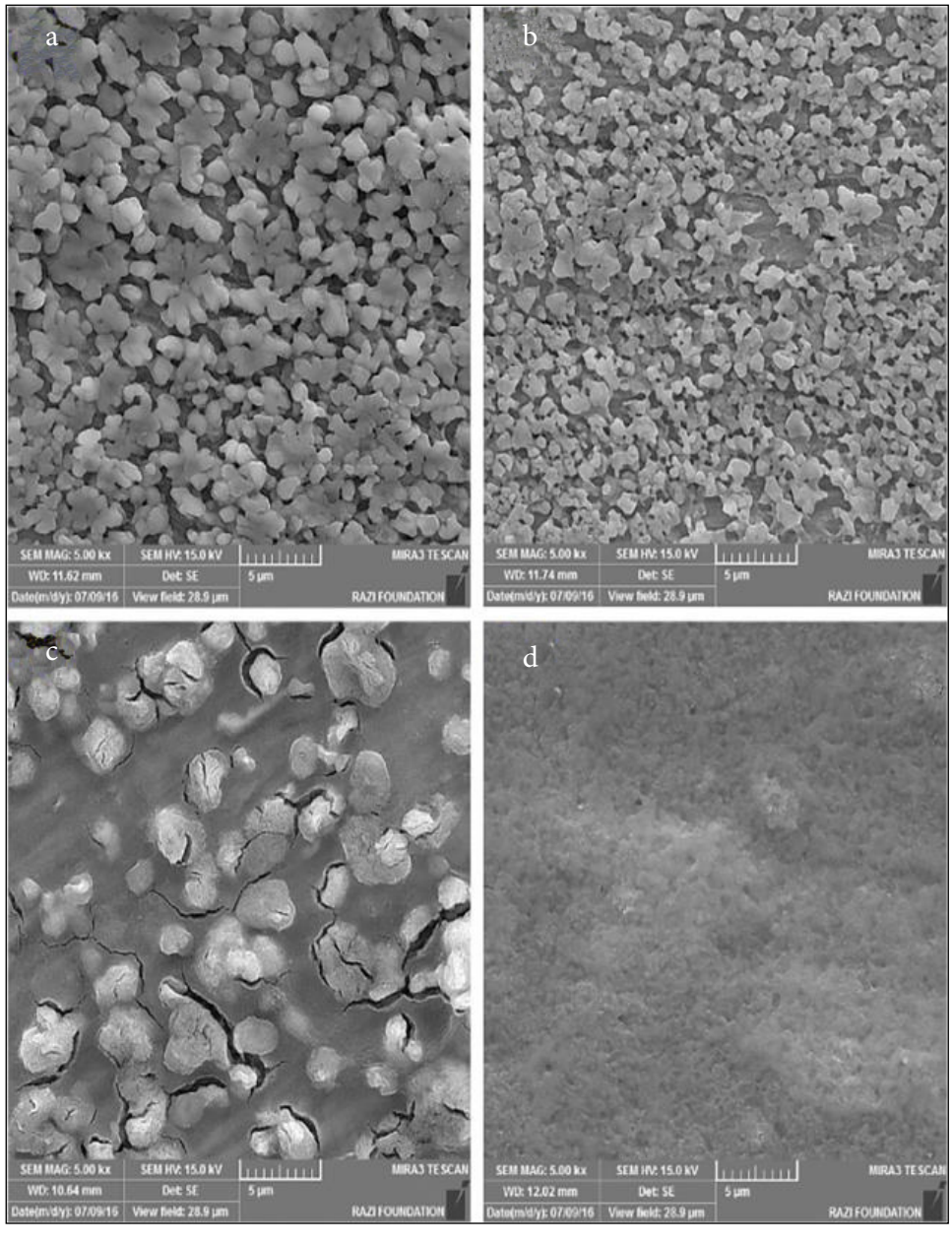

Fig. 14. SEM images of the coatings (a) CHAp, (b) Ag-CHAp, (c) Ag-1FCHAp and (d) Ag-2FCHAp [135]

(ratio of [P]/[F] was 3) showed a compact structure with small cracks. However, in the Ag-2FCHAp sample (ratio of [P]/[F] was 6), as the amount of fluoride increased, the agglomeration was omitted. It was concluded that antibacterial activity of coatings against the Gram-negative bacterium, *E. coli*, increased with increasing the amount of fluoride.

The composite coatings of titania–calcium phosphate (TiO_2–CP) have been fabricated also using sol–gel methods [113, 136, 137]. *In vitro* tests demonstrated that microporous TiO_2–CP coatings doped with Sr, Co and F possessed multiple functions of antimicrobial, angiogenic and osteogenic capabilities [136]. The composite coatings of biphasic calcium phosphate BCP/TiO_2 synthesized on the Ti alloy showed higher scratch resistance than BCP-only coating [113]. The authors concluded that the improved scratch resistance of the coating was certainly related to containing the compound of rutile–TiO_2. The presence of TiO_2 in the coating layer might have had an indirect effect on the corrosion morphology of the coatings. It was summarized that the resulting CP/TiO_2 composite coatings with a two-level surface relief could be promising for bone implantation [137].

The results presented in [138] confirmed that the silica barrier coatings enhanced the corrosion resistance of the base Mg alloy, reducing the corrosion current density in about two orders of magnitude. Additionally, the presence of Ca ions in these composite coatings promoted the formation of a discontinuous film of hydroxyapatite on the magnesium surface, indicating that those coatings could exhibit bioactive properties. The possible mechanism of formation of such composites is presented in Fig. 15.

Graphene oxide (GO) was used to build a new composite material with CHAp [140]. It was shown that CHAp nanoparticles could be intercalated with the GO sheets using in situ the sol–gel synthesis approach. For the synthesis of CHAp–GO composite at room temperature $Ca(NO_3)_2{\cdot}4H_2O$ and $(NH_4)_2HPO_4$ as Ca and P precursors, respectively, were used. A homogeneous GO–Ca^{2+} system was obtained by ultrasonic dispersion, after which a diammonium hydrogen phosphate solution was added dropwise to the system. It is interesting to note that gelation took place after 2 h of magnetic stirring at room temperature; after that, an ageing step of 2 days at 60°C was performed. It was mentioned that the interaction between CHAp nanoparticles and GO improved the bioactivity of the composite material.

Partially by the same authors it has been recently demonstrated that the sol–gel synthesis method could be successfully used for the development of minimal invasive CaP-based bionanocomposites by the incorporation of antimicrobial imidazolium IL [141]. Nanostructured IL-loaded calcium phosphate gel materials were obtained at room temperature by using the sol–gel approach.

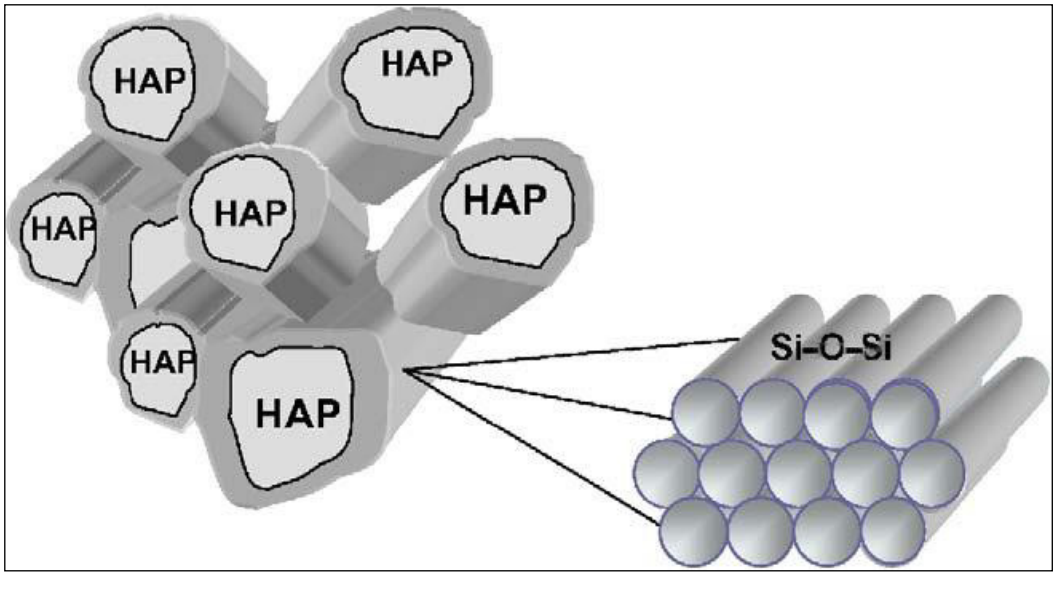

Fig. 15. Schematic illustration of the formation of silica/CHAp composite [139]

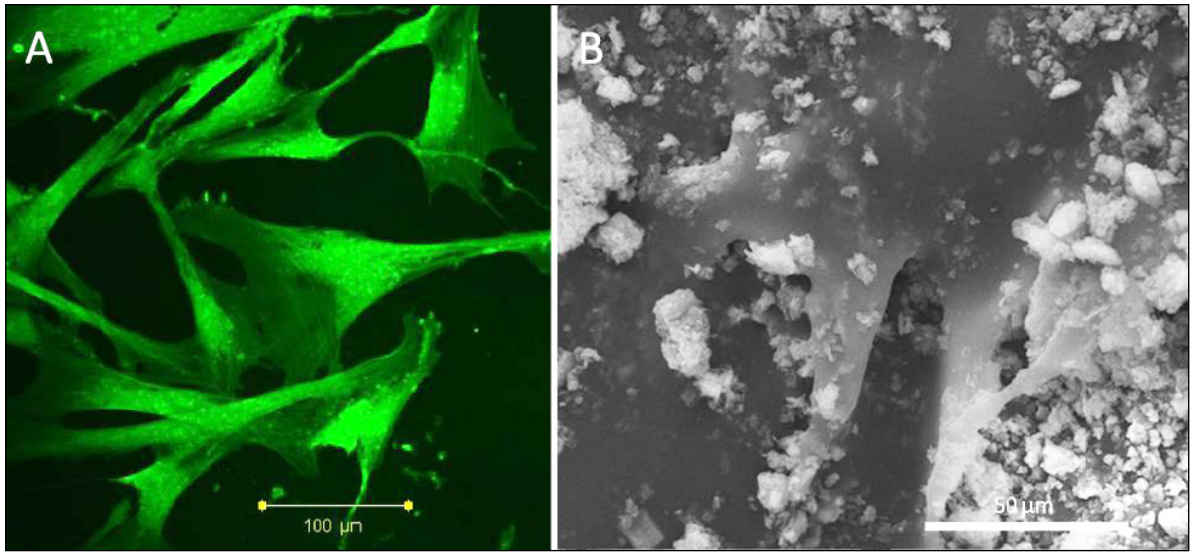

Fig. 16. Qualitative images obtained by immunofluorescence (A) and SEM (B) are representative of hMSC differentiating in osteoblast phenotype on the CaP-IL composite after day 21 of cell culture [141]

Calcium nitrate tetrahydrate and ammonium phosphate dibasic were chosen as precursors of Ca^{2+} and PO_4^{3-} ions, respectively, in a molar ratio of Ca/P in a range of 1.50–1.67. The gel transition of the IL-free system occurred after 1 h of magnetic mixing at 25°C, but the IL induced shorter gelification times. After gelification, an aging step of 2 days at 60°C was performed. The gels were deposited on coverslips and incubated with *C. albicans*. The formation of biofilms was studied by scanning electron microscopy. Biological assays were assessed using human mesenchymal stem cells (hMSCs). Qualitative images of hMSC differentiating in osteoblast phenotypes on the CaP-IL composite showed a flattened cell shape (Fig. 16). It was concluded that the optimization of IL N-alkyl chain lengths allowed modulating simultaneously biological responses, inhibiting microbial proliferation and biofilm formation, and reducing inflammatory activity. According to the authors, these CaP gels with imidazolium IL additives allowed them to overcome some issues associated with the use of antibiotic and antimicrobial nanoparticles, thus indicating that these biomaterials have the potential to avoid microbial infections and enhance bone growth in treated injuries.

CONCLUSIONS

It can be concluded from the summarized results that the sol–gel synthesis method is a very convenient synthetic technique for the fabrication of calcium hydroxyapatite and related calcium phosphate coatings and films including bioglasses and different composite materials. In most of the cases the sol–gel derived calcium phosphate-based coatings formed on different substrates are highly compact, uniform with the desired thickness and morphological features. Based on the results of the works found in these articles, there were some proposals for future research and clinical uses of the calcium phosphate biomaterials developed. The results observed during the *in vitro* and *in vivo* studies of the synthesized coatings have suggested that bone formation and tighter bone bonding occurred. The developed bioceramic coatings showed a great potential for dental and orthopedic applications. Finally, the sol–gel method has been shown to be a good way to obtain nanostructured calcium hydroxyapatite, other phosphates, bioglasses and different composite materials.

ACKNOWLEDGEMENTS

AK would like to express his sincere gratitude for the Fellowship administrated by The Japan Society for the Promotion of Science (JSPS). Fellow's ID No.: L12546.

Received 6 November 2019
Accepted 29 November 2019

References

1. M. Vallet-Regi, J. M. Gonzalez-Calbet, *Progr. Solid State Chem.*, **32**, 1 (2004).
2. D. A. Cardoso, J. A. Jansen, S. C. G. Leeuwenburgh, *J. Biomed. Mater. Res., Part B*, **100B**, 2316 (2012).
3. J. Kolmas, E. Groszyk, D. Kwiatkowska-Róhycka, *BioMed Res. Int.*, **Article ID 178123**, 1 (2014).
4. G. Tripathi, Y. Sugiura, A. Kareiva, E. Garskaite, K. Tsuru, K. Ishikawa, *J. Biomater. Appl.*, **33**, 259 (2018).
5. W. Goetz, S. N. Papageorgiou, *Current Pharmac. Biotechnol.*, **18**, 95 (2017).
6. J. T. B. Ratnayake, M. Mucalo, G. J. Dias, *J. Biomed. Mater. Res., Part B*, **105B**, 1285 (2017).
7. S. V. Dorozhkin, *Materials*, **2**, 1975 (2009).
8. A.-M. Yousefi, H. Oudadesse, R. Akbarzadeh, E. Wers, A. Lucas-Girot, *Nanotechnol. Rev.*, **3**, 527 (2014).
9. B. Ben-Nissan, A. H. Choi, D. W. Green, B. A. Latella, J. Chou, A. Bendavid, in: S. Zhang (ed.) *Biological and Biomedical Coatings Handbook: Processing and Characterization*, p. 37, CRS Press, Boca Raton, Florida (2011).
10. A. J. Salinas, M. Vallet-Regi, *RSC Adv.*, **3**, 11116 (2013).
11. M. Seyedmajidi, S. Haghanifar, K. Hajian-Tilaki, S. Seyedmajidi, *Biomed. Mater.*, **13**, 025015 (2018).
12. M. Li, P. Xiong, F. Yan, et al., *Bioact. Mater.*, **3**, 1 (2018).
13. B. Ben-Nissan, *Current Opin. Solid State Mater. Sci.*, **7**, 283 (2003).
14. B. Ben-Nissan, I. Macha, S. Cazalbou, A. H. Choi, *Nanomedicine*, **11**, 531 (2016).
15. M. Furko, K. Balazsi, C. Balazsi, *Rev. Adv. Mater. Sci.*, **48**, 25 (2017).
16. Y. C. Weng, H. X. Liu, S. P. Ji, et al., *Appl. Surf. Sci.*, **457**, 1025 (2018).
17. B. M. Hidalgo-Robatto, J. J. Aguilera-Correa, M. Lopez-Alvarez, et al., *Surf. Coat. Technol.*, **349**, 736 (2018).
18. G. Graziani, M. Boi, M. Bianchi, *Coatings*, **8**, 269 (2018).
19. A. M. Kumar, A. Y. Adesina, M. A. Hussein, et al., *Mater. Sci. Eng., C.*, **98**, 482 (2019).
20. T. Tite, A.-C. Popa, L. M. Balescu, et al., *Materials*, **11**, 2081 (2018).
21. R. Ravikrishna, M. Ren, K. T. Valsaraj, *J. Sol-Gel Sci. Technol.*, **38**, 203 (2006).
22. D. O. Costa, S. J. Dixon, A. S. Rizkalla, *ACS Appl. Mater. Interf.*, **4**, 1490 (2012).
23. I. Bogdanoviciene, A. Beganskiene, K. Tõnsuaadu, J. Glaser, H.-J. Meyer, A. Kareiva, *Mater. Res. Bull.*, **41**, 1754 (2006).
24. I. Sopyan, R. Singh, M. Hamdi, *Indian J. Chem., Sect. A: Inorg., Bio-inorg., Phys., Theor. Anal. Chem.*, **47**, 1626 (2008).
25. I. Bogdanoviciene, K. Tonsuaadu, A. Kareiva, *Polish J. Chem.*, **83**, 47 (2009).
26. H. Khireddine, S. Saoudi, S. Ziani, S. Meski, S. Meskour, *Asian J. Chem.*, **21**, 3885 (2009).
27. I. Bogdanoviciene, K. Tõnsuaadu, V. Mikli, I. Grigoraviciute-Puroniene, A. Beganskiene, A. Kareiva, *Centr. Eur. J. Chem.*, **8**, 1323 (2010).
28. I. Bogdanovičienė, A. Beganskienė, A. Kareiva, et al., *Chemija*, **21**, 98 (2010).
29. M. Kalidoss, R. Y. Basha, M. Doble, T. S. S. Kumar, *Front. Bioeng. Biotechnol.*, **7**, 126 (2019).
30. H. Podbielska, A. Ulatowska-Jarza, *Bull. Polish Acad. Sci. Techn. Sci.*, **53**, 261 (2005).
31. M. T. Dehaghani, M. Ahmadian, M. Fathi, *Int. J. Appl. Ceram. Technol.*, **12**, 867 (2015).
32. S. A. Omar, J. Ballarre, S. M. Cere, *Electrochim. Acta*, **203**, 309 (2016).
33. Y. L. Li, Q. M. Liang, C. Lin, X. Li, X. F. Chen, Q. Hu, *Mater. Sci. Eng., C*, **75**, 646 (2017).
34. N. Jmal, J. Bouaziz, *Mater. Sci. Eng., C*, **71**, 279 (2017).
35. A. Moghanian, S. Firoozi, M. Tahriri, A. Sedghi, *Mater. Sci. Eng., C*, **91**, 349 (2018).
36. J. H. Lopes, O. M. V. M. Vargas, I. O. Mazali, C. A. Bertran, *Mater. Sci. Eng., C*, **97**, 669 (2019).
37. C. J. Brinker, G. W. Scherer, *Sol-Gel Science: The Physics and Chemistry of Sol-Gel Processing*, Academic Press, London (1990).
38. S. Mann, S. L. Burkett, S. A. Davis, et al., *Chem. Mater.*, **9**, 2300 (1997).
39. A. Huczko, *Appl. Phys. A: Mater. Sci. Process.*, **70**, 365 (2000).
40. R. A. Caruso, M. Antonietti, *Chem. Mater.*, **13**, 3272 (2001).
41. B. L. Cushing, V. L. Kolesnichenko, C. J. O'Connor, *Chem. Rev.*, **104**, 3893 (2004).
42. J. D. Mackenzie, E. P. Bescher, *Acc. Chem. Res.*, **40**, 810 (2007).
43. A. A. White, S. M. Best, I. A. Kinloch, *Int. J. Appl. Ceram. Technol.*, **4**, 1 (2007).
44. C. Sanchez, C. Boissiere, D. Grosso, C. Laberty, L. Nicole, *Chem. Mater.*, **20**, 682 (2008).
45. R. Gupta, A. Kumar, *Biomed. Mater.*, **3**, 034005 (2008).
46. A. Kareiva, *Mater. Sci.–Medžiagotyra*, **17**, 428 (2011).
47. G. Brusatin, G. Della Giustina, *J. Sol-Gel Sci. Technol.*, **60**, 299 (2011).
48. E. Della Gaspera, D. Buso, A. Martucci, *J. Sol-Gel Sci. Technol.*, **60**, 366 (2010).
49. J. R. Jones, *Acta Biomater.*, **9**, 4457 (2013).
50. E. Della Gaspera, A. Martucci, *Sensors*, **15**, 16910 (2015).
51. R. B. Figueira, C. J. R. Silva, E. V. Pereira, *J. Coat. Technol. Res.*, **12**, 1 (2015).
52. X. Z. Guo, Q. L. Zhang, X. G. Ding, et al., *J. Sol-Gel Sci. Technol.*, **79**, 328 (2016).

53. D. D. Athayde, D. F. Souza, A. M. A. Silva, et al., *Ceram. Int.*, **42**, 6555 (2016).
54. A. E. Danks, S. R. Hall, Z. Schnepp, *Mater. Horizons*, **3**, 91 (2016).
55. A. Feinle, M. S. Elsaesser, N. Huesing, *Chem. Soc. Rev.*, **45**, 3377 (2016).
56. B. C. Dave, in: D. A. Glocker, S. V. Ranade (eds.), *Medical Coatings and Deposition Technologies*, p. 373, Wiley-Scrivener, Beverly (2016).
57. A. Styskalik, D. Skoda, C. E. Barnes, J. Pinkas, *Catalysts*, **7**, 168 (2017).
58. K. Zheng, A. R. Boccaccini, *Adv. Coll. Interf. Sci.*, **249**, 363 (2017).
59. M. Guglielmi, A. Martucci, *J. Sol-Gel Sci. Technol.*, **88**, 551 (2018).
60. M. C. Goncalves, *Molecules*, **23**, 2021 (2018).
61. R. Ghosh, R. Sarkar, *J. Austral. Ceram. Soc.*, **54**, 71 (2018).
62. E. Fiume, J. Barberi, E. Verne, F. Baino, *J. Funct. Biomater.*, **9**, 24 (2018).
63. D. Boudemagh, P. Venturini, S. Fleutot, F. Cleymand, *Polym. Bull.*, **76**, 2621 (2019).
64. S. Esposito, *Materials*, **12**, 668 (2019).
65. K. A. Gross, C. S. Chai, G. S. K. Kannangara, B. Ben-Nissan, L. Hanley, *J. Mater. Sci.: Mater. Med.*, **9**, 839 (1998).
66. Y. Masuda, K. Matubara, S. Sakka, *J. Ceram. Soc. Jpn.*, **98**, 1255 (1990).
67. C. S. Chai, B. Ben-Nissan, *J. Mater. Sci.: Mater. Med.*, **10**, 465 (1999).
68. D.-M. Liu, T. Troczynski, D. Hakimi, *J. Mater. Sci.: Mater. Med.*, **13**, 657 (2002).
69. F. A. Azem, A. Cakir, *J. Sol-Gel Sci. Technol.*, **51**, 190 (2009).
70. J. X. Zhang, R. F. Guan, X. P. Zhang, *J. Alloys Compd.*, **509**, 4643 (2011).
71. S. Q. Chen, Z. Q. Zhu, J. Z. Zhu, et al., *Appl. Surf. Sci.*, **230**, 418 (2004).
72. M. H. Fathi, A. Hanifi, *Adv. Appl. Ceram.*, **108**, 363 (2009).
73. Z. Stankeviciūtė, M. Malakauskaitė, A. Beganskienė, A. Kareiva, *Chemija*, **24**, 288 (2013).
74. A. Prichodko, V. Jonauske, M. Cepenko, A. Beganskiene, A. Kareiva, *Adv. Sci. Technol.*, **91**, 13 (2014).
75. M. Malakauskaite-Petruleviciene, Z. Stankeviciute, A. Beganskiene, A. Kareiva, *J. Sol-Gel Sci. Technol.*, **71**, 437 (2014).
76. H. Kheimehsari, S. Izman, M. R. Shirdar, *J. Mater. Eng. Perform.*, **24**, 2294 (2015).
77. M. Malakauskaite-Petruleviciene, Z. Stankeviciute, G. Niaura, A. Prichodko, A. Kareiva, *Ceram. Int.*, **41**, 7421 (2015).
78. M. Malakauskaite-Petruleviciene, Z. Stankeviciute, G. Niaura, E. Garskaite, A. Beganskiene, A. Kareiva, *Vibr. Spectrosc.*, **85**, 16 (2016).
79. V. Jonauskė, A. Prichodko, R. Skaudžius, A. Kareiva, *Chemija*, **27**, 192 (2016).
80. P. Usinskas, Z. Stankeviciute, A. Beganskiene, A. Kareiva, *Surf. Coat. Technol.*, **307**, 935 (2016).
81. P. Usinskas, Z. Stankeviciute, G. Niaura, G. Juodzbalys, A. Kareiva, *J. Sol-Gel Sci. Technol.*, **83**, 268 (2017).
82. V. Jonauske, S. Stanionyte, S.-W. Chen, et al., *Coatings*, **9**, 334 (2019).
83. P. Usinskas, Z. Stankeviciute, G. Niaura, J. Ceponkus, A. Kareiva, *Mater. Sci.–Medžiagotyra*, **25**, 365 (2019).
84. W. Chen, S. Oh, A. P. Ong, et al., *J. Biomed. Mater. Res., Part A*, **82A**, 899 (2007).
85. G. C. Qi, S. Zhang, K. A. Khor, et al., *Appl. Surf. Sci.*, **255**, 304 (2008).
86. A. Buyukaksoy, N. C. Koseoglu, M. H. Aslan, A. Y. Oral, *Adv. Eng. Mater.*, **11**, B77 (2009).
87. B. Hongthong, S. K. Hodak, S. Tungasmita, in: S. Suttiruengwong, W. Sricharussin (eds.), *Functionalized and Sensing Materials*, Vol. 93–94, p. 231, Trans Tech Publications, Zurich (2010).
88. Y. L. Cai, S. Zhang, X. T. Zeng, M. Qian, D. E. Sun, W. J. Weng, *Thin Solid Films*, **519**, 4629 (2011).
89. S. Samani, S. M. Hossainalipour, M. Tamizifar, H. R. Rezaie, *J. Biomed. Mater. Res., Part A*, **101**, 222 (2013).
90. B. Tian, W. Chen, Y. F. Dong, et al., *RSC Adv.*, **6**, 8549 (2016).
91. X. Feng, J. Shang, J. C. Chen, *Molec. Catal.*, **427**, 11 (2017).
92. K. S. Oh, K. J. Kim, Y. K. Jeong, et al., *Key Eng. Mater.*, **264–268**, 2107 (2004).
93. J. J. Buckley, A. F. Lee, L. Olivi, K. Wilson, *J. Mater. Chem.*, **20**, 8056 (2010).
94. N. Matsumoto, K. Sato, K. Yoshida, K. Hashimoto, Y. Toda, *Acta Biomater.*, **5**, 3157 (2009).
95. Z. Radovanovic, B. Jokic, D. Veljovic, et al., *Appl. Surf. Sci.*, **307**, 513 (2014).
96. O. Lysenko, O. Dubok, A. Borysenko, O. Shinkaruk, *J. Nanopart. Res*. **17**, Art. No. 178 (2015).
97. R. Rogojan, E. Andronescu, M. Necula, C. Cercel, R. Popescu, G. Stoian, *Roman. Biotechnol. Lett.*, **23**, 13425 (2018).
98. D. Q. Xiao, F. Yang, Q. Zhao, et al., *RSC Adv.*, **8**, 29526 (2018).
99. I. C. Pereira, A. S. Duarte, A. S. Neto, J. M. F. Ferreira, *Mater. Sci. Eng., C*, **96**, 606 (2019).
100. Y. L. Hong, H. S. Fan, B. Li, B. Guo, M. Liu, X. D. Zhang, *Mater. Sci. Eng. R Rep.*, **70**, 225 (2010).
101. D. A. Cardoso, J. A. Jansen, S. C. G. Leeuwenburgh, *J. Biomed. Mater. Res., Part B*, **100B**, 2316 (2012).
102. S. V. Dorozhkin, *Front. Nanobiomed. Res.*, **2**, 219 (2014).
103. F. Chen, Y. J. Zhu, *Current Nanosci.*, **10**, 465 (2014).
104. S. V. Dorozhkin, in: C. Liu, H. He (eds.), *Developments and Applications of Calcium Phosphate Bone Cements*, Vol. 9, p. 355, Springer, Heidelberg (2018).

105. N. A. Nawawi, I. Sopyan, S. Ramesh, Afzeri, *Asia-Pac. J. Chem. Eng.*, **6**, 823 (2011).
106. S. Basu, A. Ghosh, A. Barui, B. Basu, *ACS Biomater. Sci. Eng.*, **4**, 857 (2018).
107. S. Basu, A. Ghosh, A. Barui, B. Basu, *J. Biomater. Appl.*, **33**, 1035 (2019).
108. R. G. Tilkin, J. G. Mahy, N. Regibeau, C. Grandfils, S. D. Lambert, *ChemistrySelect*, **4**, 6634 (2019).
109. L. Gan, R. Pilliar, *Biomater.*, **25**, 5303 (2004).
110. E. Landi, G. Celotti, G. Logroscino, A. Tampieri, *J. Eur. Ceram. Soc.*, **23**, 2931 (2003).
111. Z. Stankeviciūtė, M. Malakauskaitė, A. Beganskienė, A. Kareiva, *Chemija*, **24**, 288 (2013).
112. J. Katic, M. Metikos-Hukovic, R. Babic, *J. Appl. Electrochem.*, **44**, 87 (2014).
113. B. Dikici, M. Niinomi, M. Topuz, S. G. Koc, M. Nakai, *J. Sol-Gel Sci. Technol.*, **87**, 713 (2018).
114. S. A. Adeleke, A. R. Bushroa, I. Sopyan, *Surf. Eng. Appl. Electrochem.*, **53**, 419 (2017).
115. E. A. Abou Neel, D. M. Pickup, S. P. Valappil, R. J. Newport, J. C. Knowles, *J. Mater. Chem.*, **19**, 690 (2009).
116. M. N. Rahaman, D. E. Day, B. S. Bal, et al., *Acta Biomater.*, **7**, 2355 (2011).
117. Y. M. Kim, D. H. Kim, C. W. Song, et al., *Korean J. Orthod.*, **48**, 163 (2018).
118. A. Wajda, W. H. Goldmann, R. Detsch, A. R. Boccaccini, M. Sitarz, *J. Non-Cryst. Solids*, **511**, 86 (2019).
119. X. X. Wang, S. Cai, T. L. Liu, et al., *Ceram. Int.*, **40**, 3389 (2014).
120. S. Omar, F. Repp, P. M. Desimone, et al., *J. Non-Cryst. Solids*, **425**, 1 (2015).
121. M. Catauro, F. Papale, L. Sapio, S. Naviglio, *Mater. Sci. Eng., C.*, **65**, 188 (2016).
122. S. C. Santos, L. S. Barreto, E. A. dos Santos, *J. Non-Cryst. Solids*, **439**, 30 (2016).
123. A. Moghanian, A. Sedghi, A. Ghorbanoghli, E. Salari, *Ceram. Int.* **44**, 9422 (2018).
124. K. Kaur, K. J. Singh, V. Anand, et al., *Ceram. Int.*, **42**, 12651 (2016).
125. S. Pouraghaei, F. Moztarzadeh, N. Nezafati, F. Rahmanian, *Protect. Metals Phys. Chem. Surf.*, **52**, 285 (2016).
126. A. R. Boccaccini, M. Erol, W. J. Stark, D. Mohn, Z. K. Hong, J. F. Mano, *Compos. Sci. Technol.*, **70**, 1764 (2010).
127. A. Beganskiene, Z. Stankeviciute, M. Malakauskaite, et al., in: S. Mathur, F. Hernandez-Ramirez, S. Kirihara, S. Widjaja (eds.), *Nanostructured Materials and Nanotechnology VII*, p. 1, John Wiley & Sons, Inc., Hoboken, NJ (2013).
128. R. M. Wang, K. Q. Sun, J. F. Wang, Y. F. He, P. F. Song, Y. B. Xiong, *Progr. Chem.*, **28**, 885 (2016).
129. D. Boudemagh, P. Venturini, S. Fleutot, F. Cleymand, *Polym. Bull.*, **76**, 2621 (2019).
130. E. Garskaite, L. Alinauskas, M. Drienovsky, et al., *RSC Adv.*, **6**, 72733 (2016).
131. R. Golubevas, A. Zarkov, L. Alinauskas, et al., *RSC Adv.*, **7**, 33558 (2017).
132. J. Trinkunaite-Felsen, Z. Stankeviciute, J. C. Yang, Thomas C. K. Yang, A. Beganskiene, A. Kareiva, *Ceram. Int.*, **40**, 12717 (2014).
133. A. Yelten, S. Yilmaz, *Ceram. Int.*, **45**, 15375 (2019).
134. N. Sasani, J. V. Khaki, S. M. Zebarjad, *J. Mechan. Behav. Biomed. Mater.*, **37**, 125 (2014).
135. K. Batebi, B. A. Khazaei, A. Afshar, *Surf. Coat. Technol.*, **352**, 522 (2018).
136. J. H. Zhou, L. Z. Zhao, *Sci.. Rep.*, **6**, 29069 (2016).
137. A. Y. Arbenin, E. G. Zemtsova, E. V. Orekhov, V. M. Smirnov, *Russ. J. Gener. Chem.*, **87**, 340 (2017).
138. L. M. Rueda, C. A. Hernandez, F. Viejo, A. E. Coy, J. Mosa, M. Aparicio, *Revista Metalurg.*, **52**, e075 (2016).
139. J. Andersson, S. Areva, B. Spliethoff, M. Linden, *Biomater.*, **26**, 6827 (2005).
140. M. G. Raucci, D. Giugliano, A. Longo, S. Zeppetelli, G. Carotenuto, L. Ambrosio, *J. Tissue Eng. Regener. Med.*, **11**, 2204 (2017).
141. M. G. Raucci, I. Fasolino, S. G. Pastore, et al., *ACS Appl. Mater. Interf.*, **10**, 42766 (2018).

Kunio Ishikawa, Aivaras Kareiva

KALCIO FOSFATINIŲ DANGŲ SINTEZĖS ZOLIŲ-GELIŲ METODU APŽVALGA

S a n t r a u k a

Kalcio fosfato pagrindu sukurtos biomedžiagos, ypač nanostruktūrizuotos, pasižymi dideliu biologiniu suderinamumu ir reikiamomis biologinėmis savybėmis. Stechiometrinio kalcio hidroksiapatito dangos yra plačiai naudojamos siekiant pagerinti metalinių implantų kauliniame audinyje integraciją. Tačiau šios dangos turi keletą trūkumų, kurie riboja jų sėkmingą taikymą medicinoje. Daugelyje mokslinių straipsnių buvo padaryta išvada, kad sintetinant tokias dangas zolių-gelių metodu galima išvengti trūkių dangose ir jų sluoksniavimosi. Dėmesys buvo skiriamas kalcio hidroksiapatito, kitų kalcio fosfatų, biostiklų ir kompozitų dangų ant skirtingų padėklų sintezės ypatumams ir įdomesnėms savybėms nagrinėti.

Šiame apžvalginiame straipsnyje apibendrinama naujausi įvairių kalcio fosfatinių dangų ir plonų plėvelių zolių-gelių sintezės pasiekimai; išryškinama implantų su kalcio fosfatinėmis dangomis dabartinė situacija, atskleidžiami naudojimo apribojimai ir galimybės, atviri iššūkiai ir būsimi šios biokeramikos pažangiausio taikymo scenarijai.